MATHEMATICAL BIOSCIENCES: AN INTERNATIONAL JOURNAL

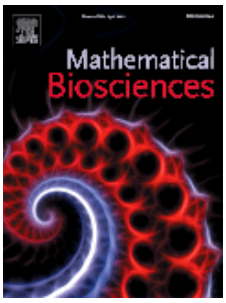

ISSN: 0025-5564

Accepted April 6th 2018

Publisher: Elsevier; Impact Factor = 1.246;

Editor: Prof. E. O. Voit (Wallace H. Coulter Dept. of Biomedical, Engineering, Georgia Tech, Atlanta, USA)

MATHEMATICAL MODELLING OF PRESSURE-DRIVEN MICROPOLAR BIOLOGICAL FLOW DUE TO METACHRONAL WAVE PROPULSION OF BEATING CILIA

N. S. Akbar[1], D. Tripathi[2#], Z. H. Khan[3] and **O. Anwar Bég[4]**

[1]DBS&H CEME, National University of Sciences and Technology, Islamabad, ***Pakistan***

[2]Dept. Mechanical Engineering, Manipal University, Jaipur-303007, ***India****.*

[3]Dept. Mathematics, University of Malakand, Chakdara, Khyber Pakhtunkhwa, ***Pakistan***

[4] Fluid Mechanics, Aeronautical and Mechanical Engineering, G77, Newton Building, University of Salford, Manchester, M54WT, ***England, UK****.*

[#]Corresponding Author-email: dharmtri@gmail.com

Abstract:

In this paper, we present an analytical study of pressure-driven flow of micropolar non-Newtonian physiological fluids through a channel comprising two parallel oscillating walls. The cilia are arranged at equal intervals and protrude normally from both walls of the infinitely long channel. A metachronal wave is generated due to natural beating of cilia and the direction of wave propagation is parallel to the direction of fluid flow. Appropriate expressions are presented for deformation via longitudinal and transverse velocity components induced by the ciliary beating phenomenon with cilia assumed to follow elliptic trajectories. The conservation equations for mass, longitudinal and transverse (linear) momentum and angular momentum are reduced in accordance with the long wavelength and creeping Stokesian flow approximations and then normalized with appropriate transformations. The resulting non-linear moving boundary value problem is solved analytically for constant micro-inertia density, subject to physically realistic boundary conditions. Closed-form expressions are derived for *axial velocity*, *angular velocity*, *volumetric flow rate* and *pressure rise*. The transport phenomena are shown to be dictated by several non-Newtonian parameters, including *micropolar material parameter and Eringen coupling parameter*, and also several geometric parameters, viz *eccentricity parameter, wave number and cilia length*. The influence of these parameters on streamline profiles (with a view to addressing trapping features via bolus formation and evolution), pressure gradient and other characteristics are evaluated graphically. Both axial and angular velocities are observed to be substantially modified with both micropolar rheological parameters and furthermore are significantly altered with increasing volumetric flow rate. Free pumping is also examined. An inverse relationship between pressure rise and flow rate is computed which is similar to that observed in Newtonian fluids. The study is relevant to hemodynamics in narrow capillaries and also bio-inspired micro-fluidic devices.

Key words: *Bio-Propulsion; Metachronal Wave; Beating Cilia; Eringen Micropolar Fluid Model; Stokesian Dynamics; Physiological Transport.*

1 INTRODUCTION

Numerous working fluids within the human body are known to be non-Newtonian. Synovial fluids [1], vitreous humour [2], reproductive liquids [3], gastric liquids [4] and blood flow in narrow capillaries [5], cerebro-spinal fluid [6] and nasal mucus [7] are only a few examples of non-Newtonian liquids which have received significant attention in biorheological studies. Building on clinical and laboratory studies [8], mathematical modelling of rheological flows in a biological context has been an active area of endeavor and has therefore emerged as a rich sub-area in its own right within modern fluid dynamics. The development of many constitutive models in initially polymer and chemical engineering since the 1940s has infiltrated into many intriguing and very diverse areas of modern biofluid mechanics. An excellent perspective of many robust formulations which have been produced and applied quite successfully, have been given periodically by leading exponents of biorheology including Thurston [9], Skalak and Goldsmith [10] and Skalak *et al*. [11]. Further expositions of recent developments in, for example, *embryological transport* are summarized in Fauci and Dillon [12]. Although there is still great popularity for deploying the more elementary rheological models e.g. power-law, Casson, Eyring-Powell and more intricate viscoelastic models e.g. Oldroyd-B, Maxwell, Rivlin-Ericksen, these models unfortunately do not provide a mechanism for simulating *micro-structural* properties of biofluids. The presence of plasma, proteins, erythrocytes, leukocytes and fats within physiological suspensions is known to contribute unique hydrodynamic properties to the performance of these fluids. Micro-rheological characteristics are therefore intrinsic to such liquids. Eringen [13] first proposed the theory of micropolar fluids to describe fluent media such as colloidal solutions, liquid crystals, fluids with additives, low concentration suspensions, blood, slurries, lubricants etc. Physically, micropolar fluids belong to a larger family of much more complex non-Newtonian fluids, namely *micromorphic fluids* which contain fluid elements with deformable microstructure, admitting intrinsic motion characteristics and possessing a *non-symmetrical* stress tensor. Extensive details of the constitutive equations for such fluids are documented in Lukaszewicz [14]. Micropolar fluids can sustain rotation with individual motions which support stress and body moments and are influenced by spin-inertia [15]. A particular advantage of the micropolar model is that the classical Navier-

Stokes model for Newtonian fluids can be retrieved as a special case by negating micropolar (vortex viscosity and spin effects). Micropolar fluids therefore provide a significantly more amenable model for computation than micromorphic fluids and can represent fluids consisting of rigid, randomly oriented (or spherical) particles suspended in a viscous medium, where the deformation of fluid particles is ignored (when deformation is important the more complex Eringen micro-stretch model is needed). In micropolar fluid dynamics, the classical continuum and thermodynamics laws are extended with additional equations, which account for the conservation of micro inertia moments and the balance of first stress moments which arise due to the consideration of micro-structure in a fluid. Hence new kinematic variables (*gyration tensor, microinertia moment tensor*), and concepts of body moments, stress moments and micro-stress are combined with classical continuum fluid dynamics theory. Micropolar theory has been utilized successfully in hemodynamics by Eringen and Kang [16], synovial lubrication by Allen and Kline [17] and Prakash and Sinha [18]. Further diverse applications include the work of Chaturani and Palanisamy [19] which examines micropolar pulsatile hemodynamics, Bhargava *et al.* [20] and Bég *et al.* [21] in biomagnetic tissue hydrodynamics. Further interesting studies in this realm include Chaube *et al.* [22] (who also considered wall slip effects) and Pandey and Tripathi [23]. Pandey and Tripathi [24] also addressed transient effects in micropolar transport in finite channels. Other studies include Tripathi *et al*. [25], Ellahi *et al.* [26] who considered thermal and mass diffusion in tapered stenosed arteries with wall suction, Akbar and Nadeem [27] who examined nanoscale effects (nano-particle Brownian diffusion and thermophoresis), and Ellahi *et al*.[28] who studied the micropolar arterial blood flow through a composite stenosis.

In numerous biological systems e.g. oesophagus, vas deferens etc, *hair-like structures* known as *cilia* (typically 10 microns in length), attached to the surfaces of vessels (and micro-organisms) aid in the propulsion of fluids at small length scales. Cilia are known to beat with a *whip-like asymmetric mechanism* which comprises both an *effective stroke* and a *recovery stroke*. Moreover, when many cilia function collectively, fluid dynamic interactions may induce beating out-of-phase, and this manifests in the generation of metachronal waves and exacerbated hydrodynamics. The specific *metachrony* is termed

symplectic (or antiplectic) when the metachronal wave is in the *same (or opposite)* direction as the effective stroke. Sleigh [29] studied the biology of cilia and flagella and discussed the propulsion of cilia as a metachronic wave, highlighting their significance in physiological propulsion. Miller [30] investigated the movement of Newtonian fluids initiated and sustained by mechanical cilia. Blake [31] extended the Sleigh model [29] from a mathematical perspective and employed a spherical envelope approach for ciliary propulsion. Khaderi *et al.* [32] reported that metachronal motion of symmetrically beating cilia establishes a *net pressure gradient in the direction of the metachronal wave*, which creates a *unidirectional flow field*. In another article, Khaderi and Onck [33] further developed a numerical model to analyze the interaction of magnetic artificial cilia with surrounding fluids in three dimensional flow. They considered cilia flow sensors and discussed their application in polycystic kidney disease treatment, summarizing the current literature on cilia and flow sensing with respect to polycystic kidney diseases and discussed how these findings correlate with various aspects of cyst formation. In this direction, many recent investigations [34; 35; 36; 37; 38; 39; 40] have been reported which consider the cilia-induced flow of various rheological fluids including Casson (viscoplastic i.e. yield stress) fluids, Jeffrey (viscoelastic) fluids, Cu-H_2O nanofluids, fractional generalized Burgers' fluids and Ostwald-de Waele power law fluids.

In many of the above investigations, a wide spectrum of scenarios has been investigated in peristaltic transport with micropolar fluids and separately other rheological flows with cilia effects – however no study has thusfar focused on combined micropolar peristaltic propulsion *with* cilia beating effects. A theoretical analysis of the *collective micropolar peristaltic pumping with metachronal wave propagation generated by cilia beating*, is therefore the objective of the present study. We consider two-dimensional incompressible micropolar fluid dynamic propulsion in an oscillating channel with the distensible walls lined with homogenous cilia structures. Lubrication theory is employed to simplify the coupled governing non-linear equations. The influence of micropolar parameters on cilia movement is evaluated carefully and furthermore geometric effects on peristaltic pumping are also elaborated. In light of this, the present work is an important contribution since it will expose readers to a more comprehensive approach for non-

Newtonian biological propulsion, specifically, the framework of Eringen micromorphic mechanics which has not been explored in biological ciliated propulsion thusfar.

2. MATHEMATICAL FORMULATION

We analyse the flow in an infinitely long channel of height, *h*, with the parallel distensible walls lined with an array of equi-spaced, two dimensional cilia of length, ε, arranged perpendicular to the walls of the channel which has width, *a*, as illustrated below in **Fig.1**. The geometry of the metachronal wave propagation in the transverse direction can be mathematically expressed as:

$$y = a + a\varepsilon \cos\left(\frac{2\pi x}{\lambda}\right). \tag{1a}$$

Sleigh [35] observed that cilia tips move in *elliptical* paths and in accordance with this, the *axial deformation* of the cilia can be mathematically expressed as:

$$x = x_0 + \varepsilon\alpha a \sin\left(\frac{2\pi x}{\lambda}\right). \tag{1b}$$

Due to cilia beating, the deformations in the translational velocity components [35], in the wave frame, are obtained as follows:

$$u_0 = -1 - \frac{\left(\frac{2\pi}{\lambda}\right)\varepsilon\alpha ac\cos\left(\frac{2\pi x}{\lambda}\right)}{1-\left(\frac{2\pi}{\lambda}\right)\varepsilon\alpha ac\cos\left(\frac{2\pi x}{\lambda}\right)}, \tag{2a}$$

$$v_0 = \frac{-\left(\frac{2\pi}{\lambda}\right)\varepsilon\alpha ac\sin\left(\frac{2\pi x}{\lambda}\right)}{1-\left(\frac{2\pi}{\lambda}\right)\varepsilon\alpha ac\sin\left(\frac{2\pi x}{\lambda}\right)}. \tag{2b}$$

The governing equations for the flow of an incompressible micropolar fluid in the absence of body force and body couple, in a wave frame of reference, following Eringen [45] are:

$$\nabla\cdot\vec{V} = 0, \tag{3}$$

$$\rho\left(\vec{V}\cdot\nabla\vec{V}\right) = -\nabla p + \kappa\nabla\times\vec{W} + (\mu+\kappa)\nabla^2\vec{V}, \tag{4}$$

$$\rho j\left(\vec{V}\cdot\nabla\vec{W}\right) = -2\kappa\vec{W} + \kappa\nabla\times\vec{V} - \gamma\left(\nabla\times\nabla\times\vec{W}\right) + \left(\alpha'+\beta'+\gamma\right)\nabla\left(\nabla\cdot\vec{W}\right). \tag{5}$$

where $\vec{V}=(v,0,u)$ and $\vec{W}=(0,\omega,0)$ are the velocity vector and the micro-rotation vector respectively, p is the fluid pressure, ρ is the micropolar fluid density j is the micro-gyration (Eringen's micro-inertia density parameter). The constants $\mu,\kappa,\alpha',\beta'$ and γ are material constants which satisfy the following inequalities: $2\mu+\kappa\geq 0,\quad \kappa\geq 0,$ $3\alpha'+\beta'+\gamma\geq 0,\quad \gamma\geq|\beta'|.$ Since the micro-rotation vector $\vec{W}$ is solenoidal, α',β' do not appear in the governing equations. It is pertinent to introduce non-dimensional parameters, which are defined as follows:

$$y=\frac{\bar{y}}{a},\ x=\frac{\bar{x}}{\lambda},\ t=\frac{c\bar{t}}{\lambda},\ v=\frac{\lambda\bar{v}}{a\ c},\ \phi=\frac{b}{a},\ u=\frac{\bar{u}}{c},$$
$$w=\frac{a}{c}\bar{w},\ p=\frac{\bar{p}a_2^2}{\lambda c\mu},\ h=\frac{\bar{h}}{a},\ \mathrm{Re}=\frac{\rho ca}{\mu},\ \beta=\frac{a}{\lambda},\quad j=\frac{\bar{j}}{a}. \tag{6}$$

Eqns. (3-5) transform as follows:

$$\frac{\partial u}{\partial x}+\frac{\partial v}{\partial y}=0, \tag{7}$$

$$\mathrm{Re}\,\beta\left(u\frac{\partial}{\partial x}+v\frac{\partial}{\partial y}\right)u=-\frac{\partial p}{\partial x}+\frac{\mu+k}{\mu}\left(\beta^2\frac{\partial^2 u}{\partial x^2}+\frac{\partial^2 u}{\partial y^2}\right)+\frac{k}{\mu}\frac{\partial w}{\partial y}, \tag{8}$$

$$\mathrm{Re}\,\beta^3\left(u\frac{\partial}{\partial x}+v\frac{\partial}{\partial y}\right)v=-\frac{\partial p}{\partial y}+\beta^2\frac{\mu+k}{\mu}\left(\beta^2\frac{\partial^2 v}{\partial x^2}+\frac{\partial^2 v}{\partial y^2}\right), \tag{9}$$

$$\rho acj\beta\left(u\frac{\partial}{\partial x}+v\frac{\partial}{\partial y}\right)w=-2kw+\frac{\gamma}{a^2}\left(\beta^2\frac{\partial^2 w}{\partial x^2}+\frac{\partial^2 w}{\partial y^2}\right)+k\left(\beta^2\frac{\partial v}{\partial x}-\frac{\partial u}{\partial y}\right), \tag{10}$$

where, $N=\dfrac{k}{(\mu+k)}$ is the Eringen coupling number $(0\leq N<1)$, $m^2=a^2k(2\mu+k)/(\gamma(\mu+k))$ is the Eringen micropolar material parameter and β is the wave number. In the limit $\kappa\to 0$ i.e., $N\to 0,$ the governing equations reduce to the classical Navier-Stokes equations. Applying lubrication theory approximations i.e. long wavelength $(\beta<<1)$ and low Reynolds number $(\mathrm{Re}\to 0)$ (i.e. Stokes flow) assumptions, Eqns. (8-10) therefore readily reduce to:

$$\frac{\partial p}{\partial y}=0, \tag{11}$$

$$\frac{\partial^2 u}{\partial y^2} + N\frac{\partial w}{\partial y} = (1-N)\frac{\partial p}{\partial x}, \tag{12}$$

$$-2w - \frac{\partial u}{\partial y} + \left(\frac{2-N}{m^2}\right)\frac{\partial^2 w}{\partial y^2} = 0\,. \tag{13}$$

The prescribed boundary conditions are imposed as:

$$\frac{\partial u}{\partial y} = 0,\ \frac{\partial w}{\partial y} = 0,\ at\ y = 0, \tag{14a}$$

$$w = 0,\ u = -1 - \frac{2\pi\varepsilon\alpha\beta\cos(2\pi x)}{1-2\pi\varepsilon\alpha\beta\cos(2\pi x)},\ at\ y = h = 1+\varepsilon\cos(2\pi x)\,. \tag{14b}$$

3. ANALYTICAL SOLUTION OF THE BOUNDARY VALUE PROBLEM

Eqns. (12), (13), together under the given boundary conditions (14 a), (14 b) admit closed-form solutions. The *axial velocity* is obtained as:

$$\begin{aligned} u(x,y) = &\left\{\frac{\cosh(my)}{m^2(N-2)\{\sinh(2hm)+\cosh(2hm)+1\}}\right\} \\ &-\sinh(my)hm(N-1)N\frac{\partial p}{\partial x}\{\sinh(hm)+\cosh(hm)\} \\ &-(N-1)N\frac{\partial p}{\partial x}\{\sinh(2hm)+\cosh(2hm)\} \\ &+m\{\sinh(my)+\cosh(my)\} \\ &\left(\begin{array}{l} -h^2mN\dfrac{\partial p}{\partial x} + h^2m\dfrac{\partial p}{\partial x} - 2hN^2\dfrac{\partial p}{\partial x} + 2hN\dfrac{\partial p}{\partial x} + mN\dfrac{\partial p}{\partial x}y^2 \\ -mNs - mN - m\dfrac{\partial p}{\partial x}y^2 + 2ms + 2m + N^2\dfrac{\partial p}{\partial x}y - N\dfrac{\partial p}{\partial x}y \end{array}\right) \end{aligned}$$

$$
\begin{aligned}
&-(N-1)N\frac{\partial p}{\partial x}\{\sinh(2my)+\cosh(2my)\}\\
&-2(N-1)N\frac{\partial p}{\partial x}\left(h^2m^2-hm^2y-1\right)\\
&\{\sinh(m(h+y))+\cosh(m(h+y))\}\\
&-m\{\sinh(2hm+my)+\cosh(2hm+my)\}\\
&\left(\begin{array}{l}
h^2mN\dfrac{\partial p}{\partial x}+h^2(-m)\dfrac{\partial p}{\partial x}-2hN^2\dfrac{\partial p}{\partial x}+2hN\dfrac{\partial p}{\partial x}-\\
mN\dfrac{\partial p}{\partial x}y^2+mNs+mN+m\dfrac{\partial p}{\partial x}y^2\\
\qquad -2ms-2m+N^2\dfrac{\partial p}{\partial x}y-N\dfrac{\partial p}{\partial x}y
\end{array}\right)\\
&-hm(N-1)N\frac{\partial p}{\partial x}\{\sinh(hm+2my)+\cosh(hm+2my)\},
\end{aligned}
\tag{15}
$$

The *microrotation (angular velocity of micro-elements) vector* emerges as:

$$
\begin{aligned}
w(x,y)=&\left[\begin{array}{l}
(N-1)\dfrac{\partial p}{\partial x}y\{\cosh(my)-\sinh(my)\}\{-m\sinh(2hm+my\}\\
\dfrac{-m\cosh(2hm+my)-m\sinh(my)-m\cosh(my)}{m(N-2)\{\sinh(2hm)+\cosh(2hm)+1)\}}
\end{array}\right]\\
&+\left[\begin{array}{l}
(N-1)\dfrac{\partial p}{\partial x}\{\cosh(my)-\sinh(my)\}\\
\{hm\sinh(hm+2my)+hm\cosh(hm+2my)\\
+hm\sinh(hm)-\sinh(2hm)+hm\cosh(hm)\\
\dfrac{-\cosh(2hm)+\sinh(2my)+\cosh(2my)\}}{m(N-2)\{\sinh(2hm)+\cosh(2hm)+1\}}
\end{array}\right],
\end{aligned}
\tag{16}
$$

where $s=\dfrac{2\pi\varepsilon\alpha\beta\cos(2\pi x)}{1-2\pi\varepsilon\alpha\beta\cos(2\pi x)}$.

The *volumetric flow rate* is computed in the wave frame courtesy of the following Eqn. as:

$$Q = \int_0^H u dy \,. \tag{17}$$

The pressure rise (Δp) *across one wavelength* can be computed by using the following expression:

$$\Delta p = \int_0^1 \left(\frac{\partial p}{\partial x} \right) dx \,. \tag{18}$$

The *stream function* in the wave frame (obeying the Cauchy-Riemann equations, $u = \frac{\partial \psi}{\partial y}$ and $v = -\frac{\partial \psi}{\partial x}$) may be computed by using Eq.(17). Visualization of streamlines is achieved with **Mathematica** symbolic software.

4. GRAPHICAL RESULTS AND DISCUSSION

Inspection of the analytical solutions (15), (16) reveals that the key control parameters for the problem examined are micropolar material parameter (m), Eringen coupling parameter (N), eccentricity parameter (α), wave number (β) and cilia length (ε). **Figs. 2-7** depict the effects of these parameters on axial velocity (u), micro-rotation component (w), pressure gradient (dp/dx), pressure rise-flow relationship and streamline profiles.

Figs.2a-c illustrate the evolution of axial velocity (u) with transverse coordinate (y) for variation in micropolar material parameter (m), Eringen coupling parameter (N) and volumetric flow rate (Q). The lower and upper walls correspond to y=0 and y = 1.7. Evidently very different responses are computed in the lower channel half space as compared with the upper channel half space. With greater micropolar material parameter, initially in the zone near the lower wall, the axial velocity (**Fig. 2a**) is damped somewhat. In this section of the channel, there is also a distinct decay in axial velocity from the maximum value at the lower wall. In this lower zone of the channel, therefore, greater micropolar effect decelerates the axial flow. Towards the channel central zone (y ~0.9), however a dramatic modification in axial velocity arises. Increasing micropolar material parameter thereafter is observed to accelerate the axial flow. Despite the alteration in

axial velocity response with micropolar effect, the descending nature of axial velocity with greater progressive distance from the lower wall is sustained. Axial velocity attains a minimal value therefore at the upper wall. The parameter *m* arises solely as an inverse quadratic function in the micro-rotation acceleration term, $+(\frac{2-N}{m^2})\frac{\partial^2 w}{\partial y^2}$ in eqn. (13). It is absent in the normalized axial momentum equation (12). There is no doubt a complex relationship between this parameter and the other micropolar rheological parameters (k, γ etc). This may be related also to the physical space available to micro-elements for rotation and also the interaction with cilia structures at the lower wall. We hypothesize that rotary motions are adjusted in such a fashion in the lower channel space that they retard the axial (translational) flow there whereas the contrary effect is generated in the upper channel half space. Nevertheless, flow reversal (backflow) is not induced anywhere in the channel since velocities are always positive. **Fig.2b** reveals that axial velocity is boosted strongly in the lower channel half space with increasing coupling parameter (N) whereas the reverse behaviour is apparent in the upper channel half space where significant deceleration accompanies greater values of N. The coupling parameter clearly arises in both the axial momentum (12) and micro-rotation (13) conservation equations. With very high N values (3, 3.2) a velocity overshoot arises near the lower wall; however, this vanishes with lower magnitudes of N. In the upper channel half space, greater N values effectively retard the axial flow. It transpires that the coupling parameter, N, has the opposite influence on axial flow development compared with the micropolar material parameter i.e. whereas the former leads to acceleration, the latter results in deceleration and vice versa. It is also evident that the curve for $N=0$ represents the axial velocity profile for Newtonian fluid (see Ref.[37]) which is a particular case of the present model. Fig.2b shows that with increasing volumetric flow rate (Q), there is a massive enhancement in axial velocity from the lower channel wall well into the upper channel half space. However, as we approach the upper channel wall the converse behaviour is witnessed. Backflow is observed at low flow rate (Q =0.5, 1.5) in the lower channel half space. Maximum axial velocity however is associated with greater flow rate (Q =5) and occurs near the lower wall.

Figs.3a-c present the influence of *m, N* and *Q* on micro-rotation component with distance across the channel. A significant deviation is computed in all plots as compared with the axial velocity distributions in Figs.2a-c. Micro-rotation (Fig.3a) i.e. *angular velocity of the micro-elements in the biofluid* is distinctly accelerated with greater micropolar material parameter (*m*) in the lower channel half space whereas it is decelerated in the upper channel half space. This is the opposite behaviour to the axial flow (Fig.2a). Stronger micropolar effect therefore encourages *spin of the micro-elements* but reduces axial flow. Weaker micropolar effect induces the contrary effect. Fig.3b shows that increasing coupling parameter, *N*, results in a strong retardation in micro-rotation in the lower channel half space, whereas it leads to substantial acceleration in the upper channel half space (i.e. faster gyratory motion of micro-elements). The effect is so strong in the lower channel space that it manifests in reverse gyratory spin (negative *w* values). The trend in Fig.3b is again in sharp contrast to the axial flow response (Fig. 2b), once again demonstrating the opposite influence of micropolar material and coupling parameters on flow characteristics. In Fig. 3c, an increase in volumetric flow rate is found to reduce micro-rotation *both at and also in close proximity* to the lower wall; however still within the lower channel wall space and for the entire upper channel half space, the opposite behaviour is induced. Strong back flow arises near the lower channel wall for all flow rates except the lowest (Q = 0.5); the peak axial velocity is computed close to the upper wall for highest flow rate (Q=5). The symmetry present in Fig.2c is lost in Fig3c; profiles are more distorted in the latter plots and the influence of flow rate on micro-rotation is less ordered than it is on axial velocity. All profiles converge to zero micro-rotation at the upper channel wall corresponding to the imposed vanishing angular velocity boundary condition there. We note that a vanishing angular velocity gradient is prescribed at the lower wall and this boundary condition, in addition to the upper wall condition, are in concurrence with standard mathematical models for micropolar fluid dynamics (see for example [17; 18; 19; 20; 21; 22; 23; 24; 25; 26; 27; 28]).

Figs.4a-b depict the pressure gradient distributions across the channel length with different values of micropolar material (*m*) and Eringen coupling (*N*) parameters. The *periodic nature of the peristaltic flow* is clearly captured in both figures. Significant peaks and troughs are observed at regular intervals. Generally, an increase in micropolar

parameter *elevates pressure gradient magnitudes* (Fig.4a). Conversely an increase in coupling parameter (Fig.4b) *only initially* enhances pressure gradient whereas subsequent elevation in *N* leads to a strong depression (the trough is amplified). The relationship between *N* and the pressure gradient is therefore more sensitive and sophisticated than that of *m*. The sensitivity is also probably strongly influenced by the cilia length although the exact interaction cannot be deduced from these figures and requires further and more detailed hydrodynamic analysis.

Figs. 5a-c illustrate the evolution of pressure rise (ΔP) with flow rate (Q) when the coupling (N), micropolar material (m) and cilia length (ε) parameters are changed. The classical inverse relationship between pressure rise and volumetric flow rate (known for Newtonian fluids) is also computed for micropolar fluids. In the *pumping region* $(\Delta P > 0)$, the pressure rise increases with greater coupling parameter (N), as observed in Fig.5a, whereas in the *augmented pumping region* $(\Delta P < 0)$ the reverse behavior is manifested. Fig. 5b indicates that greater micropolar parameter (m) results in a *decrease* in pressure rise in the pumping region and an *elevation* in the augmented pumping region. The behaviour is therefore once again the opposite of that in Fig. 5a. An increase in cilia height is observed to enhance pressure rise (Fig 5c) in the pumping region but leads to a plummet in the augmented pumping region. The so-called *free pumping region* corresponds to $\Delta P = 0$. It is known that both cilia spacing and also cilia length influence the viscous resistance per cilium and thereby also impact on the axial flow. The latter is assisted with greater cilia length and this aids in pressure rise in the lower channel half space, as observed in Fig.5c. The introduction of extra energy to the flow at the lower wall however must be compensated for by an extraction at the upper wall, and these features are also related to synchronicity of beating cilia [30]. The pressure rise is therefore found to decrease with greater cilia length in the upper channel half space. The special case of ε=0 implies *vanishing cilia* and absence of a metachronal wave. In this scenario the flow is a *purely peristaltic mechanism* due to flexibility of the walls which is studied in [23; 24].

Figs.6a-c and 7a-c present the streamline visualizations for the influence of coupling parameter, *N, and* micropolar material parameter, *m, respectively*. Significantly different

patterns are observed. With greater coupling parameter, streamlines become more separated indicating that bolus growth increases and number decreases. With greater micropolar parameter, a clear bolus appears in the vicinity of the channel centre-line (y =0); the number of boluses is also significantly greater with higher m values than higher N values. Trapping phenomena are therefore non-trivially influenced by micropolar rheology.

5. CONCLUSIONS

A theoretical investigation is presented for pressure driven peristaltic pumping of micropolar rheological biofluids in a channel comprising two parallel oscillating walls, lined with beating cilia. The metachronal wave is aligned to the axial pumping direction and is simulated via an elliptical expression. Closed-form solutions for the transformed, nonlinear boundary value problem are obtained. Interesting features are also discussed regarding bolus formation and evolution. Visualization of solutions is evaluated with symbolic software, Mathematica. The main findings of the present analysis may be summarized as:

- Axial velocity and micro-rotation (angular velocity) are respectively decreased (increased) and increased (decreased) in the lower channel and upper channel half spaces with greater Eringen micropolar parameter.
- Axial velocity and angular velocity (i.e. micro-rotation) component are respectively increased (decreased) and decreased (increased) in the lower channel and upper channel half spaces with greater values of Eringen coupling parameter.
- An inverse relationship between pressure rise and flow rate is observed for variation in all pertinent parameters e.g. coupling, micropolar material and cilia length.
- An increase in cilia height elevates pressure rise in the pumping region whereas it depresses it in the augmented pumping region.
- Increasing micropolar parameter or decreasing coupling parameter suppresses pressure rise in the pumping region and enhances it the augmented pumping region.
- The trapped bolus is a quite sensitive to changes in coupling and micropolar

parameters.

The present study is of interest in for example simulations of oesophagul transport, embryological fluid mechanics (vas deferens) and other areas of physiology. Further investigations will address alternative microstructural rheological models and will be presented imminently.

REFERENCES

[1] J. Schurz, and V. Ribitsch, Rheology of synovial fluid. Biorheology 24 (1986) 385-399.

[2] T. David, S. Smye, T. Dabbs, and T. James, A model for the fluid motion of vitreous humour of the human eye during saccadic movement. Physics in Medicine and Biology 43 (1998) 1385.

[3] P. Dunn, and B. Picologlou, Investigation of the rheological properties of human semen. Biorheology 14 (1977) 277.

[4] I. Borisov, and A. Fisher, The rheology of the gastric mucus and the secretory activity of the main gastric glands in patients with duodenal peptic ulcer. Likars' ka sprava (1992) 42-45.

[5] J.R. Castle, The rheology of abnormal human blood, Massachusetts Institute of Technology, Department of Chemical Engineering, 1964.

[6] A.A. Linninger, M. Xenos, D.C. Zhu, M.R. Somayaji, S. Kondapalli, and R.D. Penn, Cerebrospinal fluid flow in the normal and hydrocephalic human brain. IEEE Transactions on Biomedical Engineering 54 (2007) 291-302.

[7] M. Quraishi, N. Jones, and J. Mason, The rheology of nasal mucus: a review. Clinical Otolaryngology 23 (1998) 403-413.

[8] E. Roĭtman, Biorheology. Clinical hemorheology. Fundamental notions, parameters, equipment. Klinicheskaia Laboratornaia Diagnostika (2001) 25.

[9] G.B. Thurston, Effects of viscoelasticity of blood on wave propagation in the circulation. Journal of Biomechanics 9 (1976) 13-20.

[10] H. Goldsmith, and R. Skalak, Hemodynamics. Ann. Rev. Fluid Mech. 7 (1975) 213-247.

[11] R. Skalak, N. Ozkaya, and T.C. Skalak, Biofluid mechanics. Ann. Rev. Fluid Mech. 21 (1989) 167-200.

[12] L.J. Fauci, and R. Dillon, Biofluidmechanics of reproduction. Ann. Rev. Fluid Mech. 38 (2006) 371-394.

[13] A.C. Eringen, Simple microfluids. International Journal of Engineering Science 2 (1964) 205-217.

[14] G. Lukaszewicz, Micropolar Fluids: Theory and Applications, Springer Science & Business Media, 1999.

[15] O.Anwar Bég, R. Bhargava, and M. Rashidi, Numerical Simulation in Micropolar Fluid Dynamics. Lambert, Saarbrucken, Germany (2011).

[16] C. Kang, and A. Eringen, The effect of microstructure on the rheological properties of blood. Bulletin of Mathematical Biology 38 (1976) 135-159.

[17] S. Allen, and K. Kline, Lubrication theory for micropolar fluids, ASME J Applied Mech. (1971) 38(3), 646-650.
[18] J. Prakash, and P. Sinha, Lubrication theory for micropolar fluids and its application to a journal bearing. International Journal of Engineering Science 13 (1975) 217-232.
[19] P. Chaturani, and V. Palanisamy, Microcontinuum model for pulsatile blood flow through a stenosed tube. Biorheology 26 (1988) 835-846.
[20] R. Bhargava, O.Anwar Bég, S. Sharma, and J. Zueco, Finite element study of nonlinear two-dimensional deoxygenated biomagnetic micropolar flow. Communications in Nonlinear Science and Numerical Simulation 15 (2010) 1210-1223.
[21] O. Anwar Bég, R. Bhargava, S. Rawat, K. Halim, and H.S. Takhar, Computational modeling of biomagnetic micropolar blood flow and heat transfer in a two-dimensional non-Darcian porous medium. Meccanica 43 (2008) 391-410.
[22] M. Chaube, S. Pandey, and D. Tripathi, Slip effect on peristaltic transport of micropolar fluid. Appl. Math. Sci 4 (2010) 2015-2117.
[23] S. Pandey, and D. Tripathi, A mathematical model for peristaltic transport of micro-polar fluids. Applied Bionics and Biomechanics 8 (2011) 279-293.
[24] S.K. Pandey, and D. Tripathi, Unsteady peristaltic flow of micro-polar fluid in a finite channel. Zeitschrift für Naturforschung A 66 (2011) 181-192.
[25] D. Tripathi, M. Chaube, and P. Gupta, Stokes flow of micro-polar fluids by peristaltic pumping through tube with slip boundary condition. Applied Mathematics and Mechanics 32 (2011) 1587-1598.
[26] R. Ellahi, S. Rahman, S. Nadeem, and N.S. Akbar, Influence of heat and mass transfer on micropolar fluid of blood flow through a tapered stenosed arteries with permeable walls. Journal of Computational and Theoretical Nanoscience 11 (2014) 1156-1163.
[27] N.S. Akbar, and S. Nadeem, Peristaltic flow of a micropolar fluid with nano particles in small intestine. Applied Nanoscience 3 (2013) 461-468.
[28] R. Ellahi, S. Rahman, M.M. Gulzar, S. Nadeem, and K. Vafai, A mathematical study of non-Newtonian micropolar fluid in arterial blood flow through composite stenosis. Applied Mathematics & Information Sciences 8 (2014) 1567.
[29] M.A. Sleigh, The Biology of Cilia and Flagella, MacMillan, New York (1962).
[30] C. Miller, An investigation of the movement of Newtonian liquids initiated and sustained by the oscillation of mechanical cilia, Aspen Emphysema Conference, Colorado, USA (1966) 309-321.
[31] J. Blake, A spherical envelope approach to ciliary propulsion. Journal of Fluid Mechanics 46 (1971) 199-208.
[32] S. Khaderi, J. den Toonder, and P. Onck, Fluid flow due to collective non-reciprocal motion of symmetrically-beating artificial cilia. Biomicrofluidics 6 (2012) 014106.
[33] S. Khaderi, and P. Onck, Fluid–structure interaction of three-dimensional magnetic artificial cilia. Journal of Fluid Mechanics 708 (2012) 303-328.
[34] N.S. Akbar, D. Tripathi, O.A. Bég, and Z. Khan, MHD dissipative flow and heat transfer of Casson fluids due to metachronal wave propulsion of beating cilia with

thermal and velocity slip effects under an oblique magnetic field. Acta Astronautica 128 (2016) 1-12.
[35] K. Maqbool, S. Shaheen, and A. Mann, Exact solution of cilia induced flow of a Jeffrey fluid in an inclined tube. SpringerPlus 5 (2016) 1379.
[36] N.S. Akbar, D. Tripathi, Z.H. Khan, and O.A. Bég, Mathematical model for ciliary-induced transport in MHD flow of Cu-H 2 O nanofluids with magnetic induction. Chinese Journal of Physics 55 (2017) 947-962.
[37] N.S. Akbar, A.W. Butt, D. Tripathi, and O.A. Bég, Physical hydrodynamic propulsion model study on creeping viscous flow through a ciliated porous tube. Pramana 88 (2017) 52.
[38] K. Maqbool, A. Mann, A. Siddiqui, and S. Shaheen, Fractional generalized Burgers' fluid flow due to metachronal waves of cilia in an inclined tube. Advances in Mechanical Engineering 9 (2017) 1687814017715565.
[39] A. Farooq, and A. Siddiqui, Mathematical model for the ciliary-induced transport of seminal liquids through the ductuli efferentes. International Journal of Biomathematics 10 (2017) 1750031.
[40] S. Maiti, and S. Pandey, Rheological fluid motion in tube by metachronal waves of cilia. Applied Mathematics and Mechanics 38 (2017) 393-410.

FIGURES

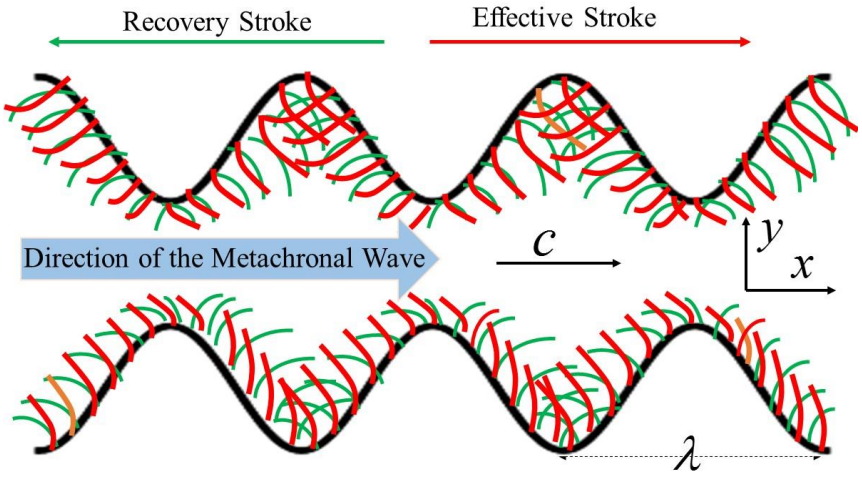

Fig 1. Geometric representation of micropolar fluid flow induced by metachronal wave propulsion.

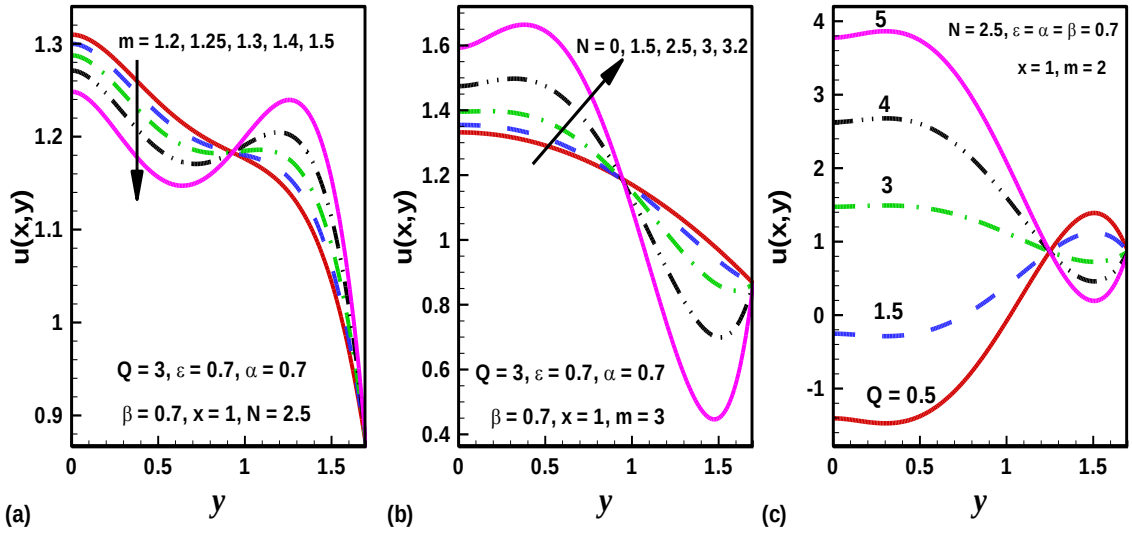

Fig.2. Axial velocity response for different physical parameters **(a)** Micro rotation parameter (*m*) **(b)** Coupling parameter (*N*) **(c)** Flow rate (*Q*)

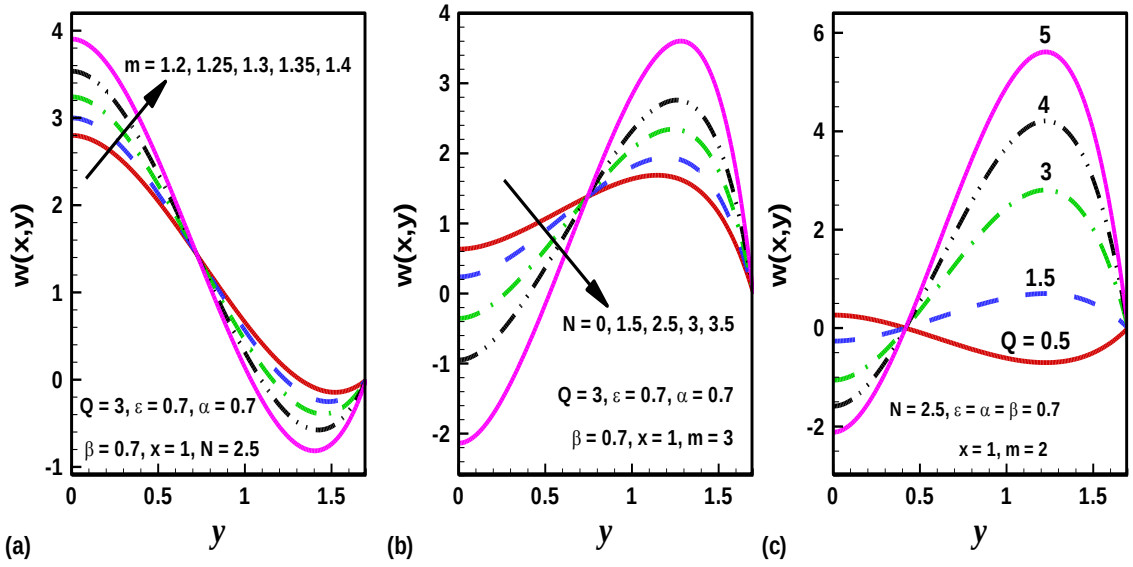

Fig.3. Microrotation component for for different physical parameters **(a)** Micro rotation parameter (*m*) **(b)** Coupling parameter (*N*) **(c)** Volumetric flow rate (*Q*).

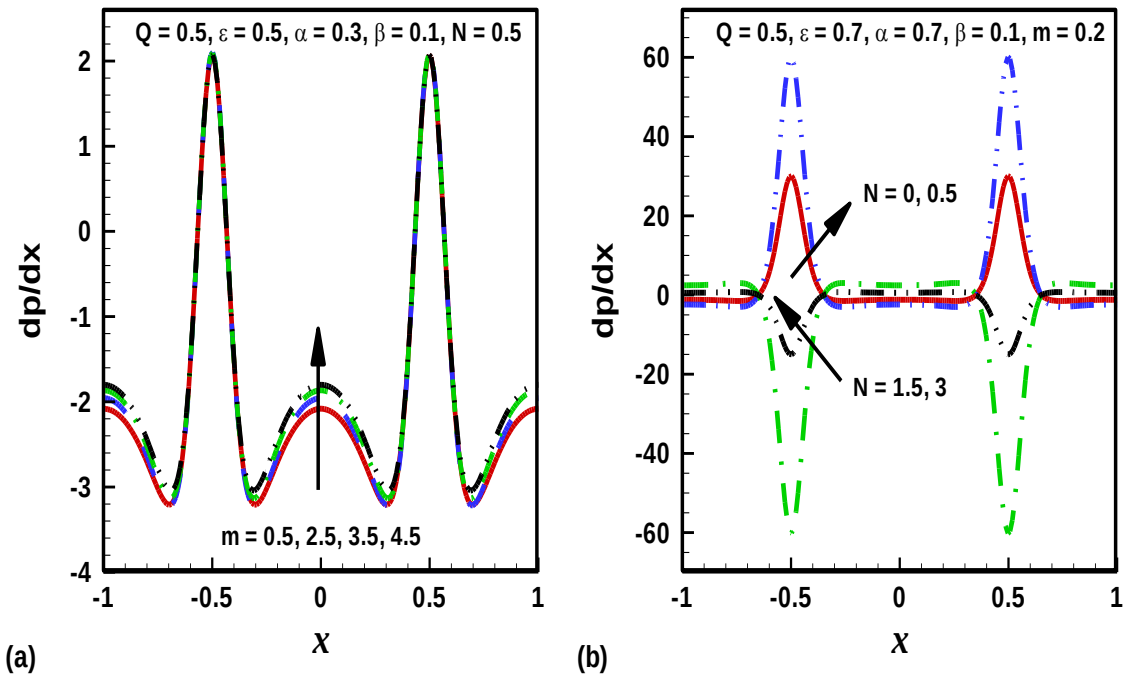

Fig. 4. Pressure gradient versus axial coordinate for different physical parameters **(a)** Micro rotation parameter (*m*) **(b)** Coupling parameter (*N*)

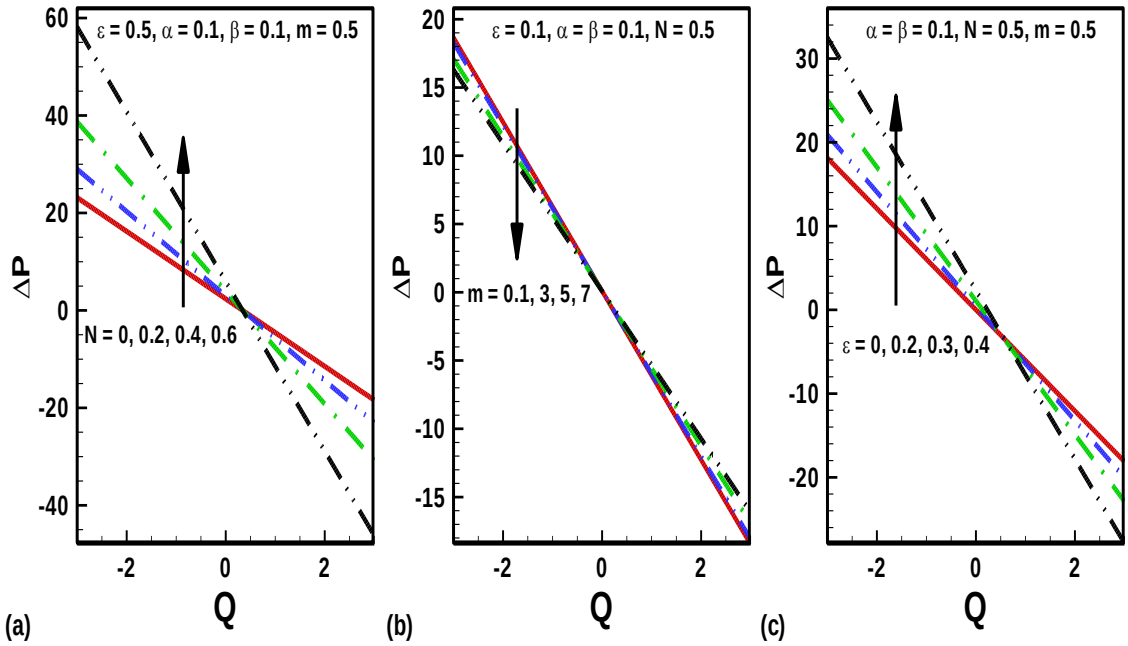

Fig.5. Pressure rise versus volumetric flow rate for different physical parameters **(a)** Micro rotation parameter (*m*) **(b)** Coupling parameter (*N*) **(c)** cilia length (*ε*)

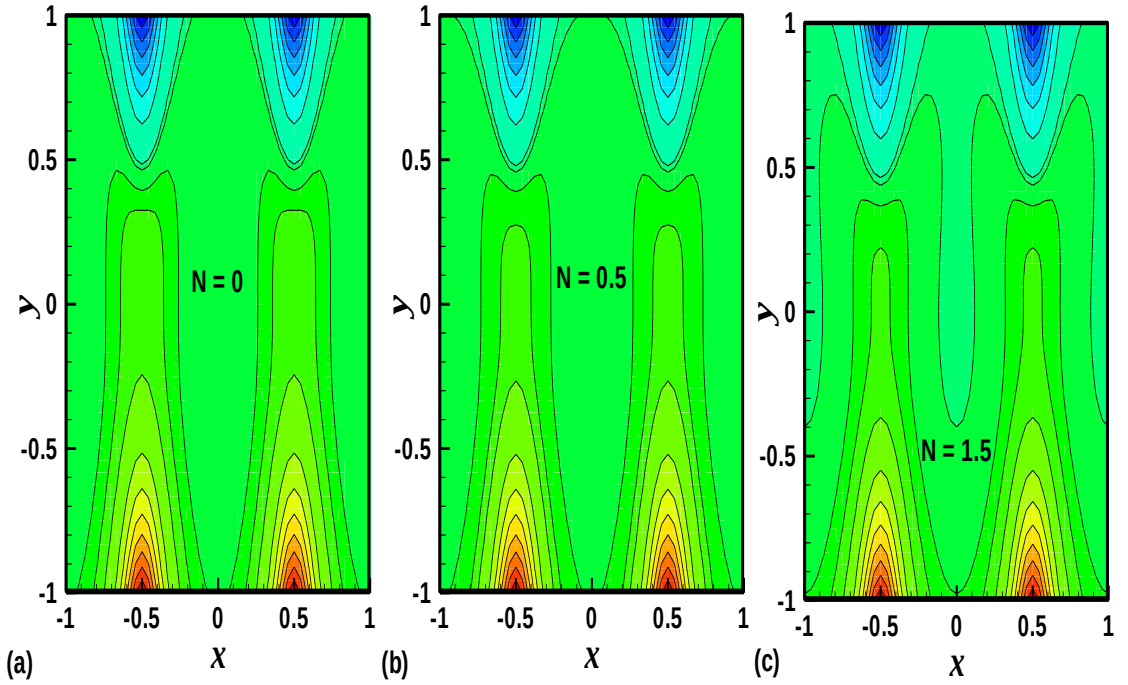

Fig.6. Streamlines for various coupling parameters with $Q = 0.5$, $\alpha = 0.1 = \beta$, $m = 0.3$, $\varepsilon = 0.3$.

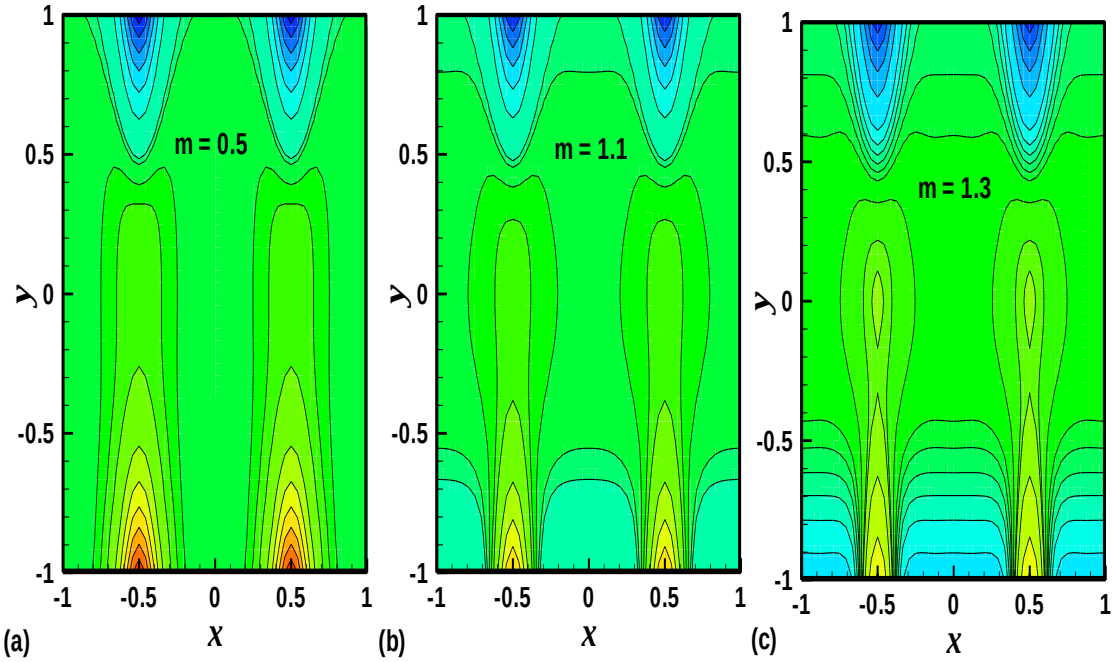

Fig.7. Streamlines for various micropolar material parameter (*m*) values with $Q = 0.5$, $\alpha = 0.1 = \beta$, $N = 0.3$, $\varepsilon = 0.3$.